

## Description of light-ion collisions in the time-dependent cluster model

W. Bauhoff

*Theoretische Kernphysik, Universität Hamburg, D-2000 Hamburg, Federal Republic of Germany*

E. Caurier and B. Grammaticos\*

*Laboratoire de Physique Nucléaire Théorique, Centre de Recherches Nucléaires Strasbourg,  
F-67037 Strasbourg Cedex, France*

M. Ploszajczak

*Niels Bohr Institute, DK-2100 Copenhagen Ø, Denmark  
and Institute of Nuclear Physics, PL-31-342 Kraków, Poland*

(Received 28 March 1985)

The time-dependent cluster model is applied to the description of light-ion reactions of various types. Special emphasis is placed on the quantitative description of the fusion excitation function in the  $^{12}\text{C}$ - $^{12}\text{C}$  system and the qualitative discussion of  $l$  matching for different binary reactions in the  $^{12}\text{C}$ - $^{16}\text{O}$  system. The Euler-Lagrange equations of the time-dependent cluster model are generalized to the multideterminantal case, and in this form they are applied to describe the evolution of parity-projected wave functions in the  $\alpha$ - $^{12}\text{C}$  reaction. For this reaction, the results for various assumptions about the trial wave function and the initial geometry of the reaction are qualitatively discussed.

### I. INTRODUCTION

One of the most important problems of theoretical physics is the understanding of the properties of many-body systems in terms of the underlying interactions between particles. Recent interest of nuclear physicists in this field was stimulated by the progress in applications of mean-field methods to the dynamics of heavy-ion collisions, in particular to a qualitative description of various inclusive properties, bound state energies, and the fission process. (For a detailed discussion of this subject we refer the reader to recent review articles.<sup>1,2</sup>) Time-dependent Hartree-Fock (TDHF) calculations with density-dependent effective Hamiltonians are sufficiently accurate to account in many cases for the experimental cross section in fusion and deep-inelastic collisions at energies above the interaction barrier. Moreover, various scattering observables are obtained by calculating the expectation values of one-body operators. In an extreme one-body approach like the one provided by the TDHF method, a calculation of average properties of the process should in principle be a meaningful procedure. In this way, e.g., the charge and mass distribution could be extracted from the nucleonic density distribution in the final state. Starting from the concept of a trajectory, the classical differential cross section has been calculated. The contact with a vast amount of data could be achieved by comparison of calculated kinetic energies and scattering angles with experimental Wilczyński plots.<sup>3</sup> Although precise quantitative criteria for the validity of the TDHF method are still lacking, one can reasonably assume that the theory is valid in heavy nuclei for low energy processes. In the collisions between light ions, the absence of a proper separation of the c.m. motion makes the application of the

TDHF method questionable, particularly at small energies above the interaction barrier. The inclusion of the spurious center-of-mass kinetic energy in TDHF leads to errors<sup>2</sup> of the order of 130 MeV/nucleon which is a small number in heavy nuclei, but not negligible in a system like, e.g.,  $^{12}\text{C}$ - $^{12}\text{C}$ , especially just above the barrier. It seems that for these light nuclei  $\alpha$  clustering plays an important role both in the ground state and in excited states. Qualitative arguments based on the binding energy of the  $\alpha$  particle in a nucleus suggest that  $\alpha$  clustering becomes unimportant in heavier nuclei. However, even in these nuclei the experimental ratios for the emission of nucleons, deuterons, tritons, and  $\alpha$  particles seem to indicate that the large preformation factor for heavier fragments in the nuclear surface cannot be described in the extreme single-particle picture.<sup>4</sup>

These difficulties can be removed in the time-dependent cluster model (TDCM) which provides an approximation to the general mean-field theory. In this model one assumes that the nucleus is built out of alpha-like clusters which are arranged in space according to a geometrical pattern determined variationally. The success of the static cluster model<sup>5</sup> has encouraged its extension to the time-dependent case.<sup>6,7</sup> We would like to emphasize that in the TDCM we take effectively into account the four-body correlations, but only in the mean field, i.e., the wave function remains a Slater determinant for all times. Our approach has thus little in common with the  $\exp\{S\}$  formulation.<sup>2</sup> The main advantage of this model is that the wave function is known analytically. The only dynamical variables are the size and the position of the clusters, the time evolution of which is governed by classical looking Euler-Lagrange equations of motion. One obtains therefore quite simple expressions and, at least for lighter nu-

clei, the model is almost analytically soluble. This apparent simplicity of the TDCM allows one to investigate a less restrictive initial geometry of the reaction than is customary in the TDHF approximation. In this latter case, even in the most elaborate calculations with three spatial dimensions, one assumes symmetry in the reaction plane and spherical initial configurations of the fragments. One should remark that the spurious c.m. motion can be separated exactly from the TDCM evolution and, moreover, no arbitrary confinement of the wave function in a box has to be introduced, as is imposed by the discretization of the single-particle wave function in the TDHF approach. On the other hand, some of the richness of the full TDHF wave function is lost in the TDCM, although the parametrization is still sufficiently rich so as to describe a great variety of nuclear phenomena, as will be demonstrated in this paper. The simplicity of the TDCM allows furthermore a straightforward extension to a multideterminantal approximation of the wave function. Below we present an application of the two-determinantal version of the model to the evolution of parity-projected cluster wave functions.

In Sec. II we present the derivation of the equations of motion in the TDCM both in the most general case of the multideterminantal wave function and in the special case of a single-determinantal approximation as reported in our earlier work.<sup>7</sup> Section III is devoted to the qualitative comparison of trajectories and various final states for the  $\alpha$ - $^{12}\text{C}$  system in different approximations: with parity-projected or parity-mixed wave functions with a variable or a frozen size of the  $\alpha$  clusters. All results have been obtained with the finite range Brink-Boeker interaction<sup>8</sup> supplemented with the Coulomb force. In Sec. IV we show the fusion excitation function for the  $^{12}\text{C}$ - $^{12}\text{C}$  system and discuss the role of various assumptions about the geometrical orientation of the two fragments in the initial state. Section V deals with the energy and angular momentum dependence of incomplete fusion processes in the reaction  $^{12}\text{C}$ - $^{16}\text{O}$ . We find that with increasing energy of the colliding ions one can follow in the TDCM a sequence of incomplete fusion or deep inelastic processes. So for more peripheral collisions of  $^{12}\text{C}$  and  $^{16}\text{O}$  we find an angular momentum selectivity for binary reactions, in qualitative agreement with predictions of the "bin model" by Wilczyński *et al.*<sup>9,10</sup> These calculations are performed only in the frozen cluster approximation, which excludes a quantitative comparison of calculated threshold angular

momenta for different binary reactions with the predictions of this model. Finally, Sec. VI summarizes the main results of the paper.

## II. THE TDCM FORMALISM

In this section we discuss essentials of the TDCM equations. In particular, we review the equations of motion for the time-dependent parity-projected cluster wave function and show the method for separating the c.m. motion.

### A. Derivation of the TDCM

The most transparent way of deriving the TDCM equations is to start with the Schrödinger time-dependent variational principle for un-normalized wave functions  $|\Phi\rangle$ :

$$\delta I = \delta \int_{t_1}^{t_2} \left\{ \frac{\langle \Phi | (i\hbar \partial_t - \hat{H}) | \Phi \rangle}{\langle \Phi | \Phi \rangle^{1/2}} \right\} dt = 0, \quad (1)$$

where  $\hat{H}$  is the nuclear many-body Hamiltonian. The variations  $\langle \delta\Phi |$  are such that

$$\langle \delta\Phi(\mathbf{r}; t_1) | = \langle \delta\Phi(\mathbf{r}; t_2) | = 0.$$

(Variations with respect to  $|\Phi\rangle$  lead to the conjugate set of equations.) From Eq. (1) one obtains the equations

$$i\hbar \{ \mathcal{N}^{-1} \partial_t - \mathcal{N}^{-2} \langle \Phi | \partial_t | \Phi \rangle \} |\Phi\rangle = \delta_{\Phi} (\mathcal{H} \mathcal{N}^{-1}) |\Phi\rangle, \quad (2)$$

where

$$\left\{ \begin{array}{c} \mathcal{N} \\ \mathcal{H} \end{array} \right\} = \left\langle \Phi \left| \left\{ \begin{array}{c} \hat{1} \\ \mathcal{H} \end{array} \right\} \right| \Phi \right\rangle. \quad (3)$$

Up to now the wave function  $\Phi$  has not yet been specified. In the following, we assume that the time evolution of  $\Phi$  is described by a set of dynamical variables  $\{q \equiv [q_1, \dots, q_{2N}]\}$ . Hence,

$$|\Phi(\mathbf{r}; t)\rangle \equiv |\Phi(\mathbf{r}; \mathbf{q}(t))\rangle, \quad (4)$$

with

$$\delta\Phi = \sum_{\alpha} (\partial_{q_{\alpha}} \Phi) \delta q_{\alpha}, \quad \partial_t \Phi = \sum_{\alpha} (\partial_{q_{\alpha}} \Phi) (\partial_t q_{\alpha}). \quad (5)$$

Consequently, Eq. (2) can now be transcribed to an equation for the  $q$ 's:

$$i\hbar \sum_{\beta} \mathcal{N}^{-1} \{ \langle \partial_{q_{\alpha}} \Phi | \partial_{q_{\beta}} \Phi \rangle - \langle \partial_{q_{\beta}} \Phi | \partial_{q_{\alpha}} \Phi \rangle + \mathcal{N}^{-1} [ \langle \partial_{q_{\beta}} \Phi | \Phi \rangle \langle \Phi | \partial_{q_{\alpha}} \Phi \rangle - \langle \partial_{q_{\alpha}} \Phi | \Phi \rangle \langle \Phi | \partial_{q_{\beta}} \Phi \rangle ] \} (\partial_t q_{\beta}) = \partial_{q_{\alpha}} (\mathcal{H} \mathcal{N}^{-1}). \quad (6)$$

Following the notation of Kerman and Koonin,<sup>11</sup> one can introduce the Lagrange bracket:

$$S_{\alpha\beta} \equiv \{q_{\alpha}, q_{\beta}\} \equiv i\hbar \mathcal{N}^{-1} \{ \langle \partial_{q_{\alpha}} \Phi | \partial_{q_{\beta}} \Phi \rangle - \langle \partial_{q_{\beta}} \Phi | \partial_{q_{\alpha}} \Phi \rangle + \mathcal{N}^{-1} [ \langle \partial_{q_{\beta}} \Phi | \Phi \rangle \langle \Phi | \partial_{q_{\alpha}} \Phi \rangle - \langle \partial_{q_{\alpha}} \Phi | \Phi \rangle \langle \Phi | \partial_{q_{\beta}} \Phi \rangle ] \}. \quad (7)$$

In this notation, the Euler-Lagrange equations (6) take the form

$$\sum_{\beta} S_{\alpha\beta} \partial_t q_{\beta} = \partial_{q_{\alpha}} (\mathcal{H} \mathcal{N}^{-1}). \quad (8)$$

If the parameters  $\mathbf{q} \equiv [q_1, \dots, q_{2N}]$  are chosen such that  $\mathbf{q} \equiv [\rho_1, \dots, \rho_N; \pi_1, \dots, \pi_N]$ , where  $(\rho_\alpha, \pi_\alpha)$ ,  $\alpha = 1, \dots, N$  represent a pair of canonical conjugate variables, then Eqs. (8) take the form of classical Hamiltonian equations. Equations (8) hold also for multideterminantal wave functions:

$$|\Phi(\mathbf{r}; t)\rangle = \sum_i f_i |\bar{\Phi}_i(\mathbf{r}; \mathbf{q}(t))\rangle, \quad (9)$$

with weight factors  $f_i$  which are constant in time.

In practical applications it is convenient to replace the real-valued variational vector  $[q_1, \dots, q_{2N}]$  by a complex-valued one  $\mathbf{q} = \mathbf{r} + i\mathbf{p}$ , where  $\mathbf{r} \equiv [r_1, \dots, r_N]$ ,  $\mathbf{p} \equiv [p_1, \dots, p_N]$ . In this case,  $|\bar{\Phi}_i(\mathbf{r}, t)\rangle \equiv |\bar{\Phi}_i(\mathbf{r}, \mathbf{q}(t))\rangle$ ,  $\langle \bar{\Phi}_i(\mathbf{r}, t) | \equiv \langle \bar{\Phi}_i(\mathbf{r}, \mathbf{q}^*(t)) |$ , and the state vector derivatives in the definition of the Lagrange bracket (7) can be replaced by derivatives of the norm. Inserting (9) in expression (1) or (6), one obtains:

$$\sum_\beta \left\{ \sum_i \mathcal{N}^{(i)} B_{\alpha\beta}^{(i)} + \mathcal{N}^{-1} \sum_{i < j} \mathcal{N}^{(i)} \mathcal{N}^{(j)} (A_\alpha^{(i)} - A_\alpha^{(j)})^* (A_\beta^{(i)} - A_\beta^{(j)}) \right\} \partial_i q_\beta = \sum_i \mathcal{N}^{(i)} \partial_{q_\alpha^*} \mathcal{X}^{(i)} + \mathcal{N}^{-1} \sum_{i < j} \mathcal{N}^{(i)} \mathcal{N}^{(j)} (A_\alpha^{(i)} - A_\alpha^{(j)})^* (\mathcal{X}^{(i)} - \mathcal{X}^{(j)}), \quad (10)$$

where

$$\left\{ \frac{\mathcal{N}}{\mathcal{X}} \right\} = \sum_{k,l} f_k f_l \langle \bar{\Phi}_k \left| \left| \frac{\hat{1}}{\hat{H}} \right| \right| \bar{\Phi}_l \rangle, \quad (11)$$

$$\left\{ \frac{\mathcal{N}^{(k)}}{\mathcal{X}^{(k)}} \right\} = \sum_l f_k f_l \langle \bar{\Phi}_k \left| \left| \frac{\hat{1}}{\hat{H}} \right| \right| \bar{\Phi}_l \rangle, \quad (12)$$

and  $A_\alpha^{(i)}$ ,  $B_{\alpha\beta}^{(i)}$  denote the derivatives

$$A_\alpha^{(i)} = (\partial_{q_\alpha} \mathcal{N}^{(i)}) / \mathcal{N}^{(i)}, \quad B_{\alpha\beta}^{(i)} = \partial_{q_\alpha^*} A_\beta^{(i)}. \quad (13)$$

The generalization of Eq. (8) to continuous representations  $\bar{\Phi}_\alpha$  such that

$$\Phi(\mathbf{r}; t) = \int f_\alpha \bar{\Phi}_\alpha(\mathbf{r}; \mathbf{q}(t)) d\alpha$$

is straightforward and will not be discussed here.

### B. Alpha clustering in light nuclei

A particularly flexible description of spatial four-particle correlations in light  $4N$  nuclei is provided by the static cluster model.<sup>5</sup> Most of the successful applications of this model have been done with simple effective interactions like those of Volkov<sup>12</sup> or Brink-Boeker.<sup>8</sup> For the ground state properties the accuracy of the cluster model is comparable to Hartree-Fock results.<sup>13</sup> The model is also able to describe excited  $\alpha$ -cluster configurations and their stability against  $\alpha$  emission, which may be important for understanding the intermediate structures in heavy ion-collisions. In Table I we compare the experimental and calculated binding energies and rms radii for a few nuclei. The theoretical results have been obtained with the  $B1$  force.<sup>8</sup> One notices that the  $B1$  force underbinds the heavier nuclei, but that nevertheless the energies of  $^{24}\text{Mg}$  and  $^{28}\text{Si}$  relative to the energies of two  $^{12}\text{C}$  and  $^{16}\text{O}$  are well reproduced. A similar underbinding for  $^{12}\text{C}$  is also obtained in the Hartree-Fock calculation<sup>14</sup> with the local version of the Skyrme force<sup>15</sup> ( $S1$ ). In heavier nuclei the density dependence contained in the Skyrme force allows one to reproduce the experimental binding energies and radii.

It is an open question how strong the  $\alpha$  clustering in light nuclei actually is. Unfortunately, the answer to this question depends sensitively on the choice of interaction as well as on the approximation for the wave function. The  $B1$  force gives strong clustering for both unprojected and angular momentum (parity) projected wave functions.<sup>16</sup> Hence,  $\alpha$ -cluster correlations for this force are largely independent of the choice of the variational wave functions. In contrast, Skyrme calculations based on unprojected wave functions give in  $^{12}\text{C}$  and  $^{16}\text{O}$  essentially no  $\alpha$  clustering. Clustering becomes visible only in parity-projected calculations<sup>16,17</sup> and, in particular, if both parity and angular momentum projection are performed before variation.<sup>16</sup> In this latter limit, the predictions of the cluster model for  $B1$  and Skyrme forces are in qualitative agreement.

The situation looks less promising for the excited states of  $^{12}\text{C}$  and  $^{16}\text{O}$ . The cluster calculations with the  $B1$  force reproduce the energies of  $\alpha$ -cluster configurations very well independently whether or not the parity and (or) angular momentum projection is performed in the trial wave function. In contrast, cluster calculations with the Skyrme force fail in all approximations.<sup>16</sup> A particularly bad agreement with the data is found for wave functions which violate both rotational symmetry and parity. Thus, we may conclude that the Skyrme force is badly suited to describe properties of excited states in light nuclei. The  $B1$  calculations, in contrast, are accurate even for the unprojected wave function.

TABLE I. The experimental and calculated energies and rms radii for nuclei investigated in this work. Results for  $^{12}\text{C}$  and  $^{24}\text{Mg}$  are taken from Ref. 18.

Nucleus	Energy (MeV)		rms radius (fm)	
	Expt.	Theory	Expt.	Theory
$^4\text{He}$	28.3	28.2	1.71	1.72
$^{12}\text{C}$	92.2	62.0	2.37	2.68
$^{16}\text{O}$	127.6	94.4	2.72	2.68
$^{24}\text{Mg}$	198.3	131.8	3.02	3.18
$^{28}\text{Si}$	236.5	157.1	3.10	3.32

### C. The TDCM formalism for the $\alpha$ -cluster model

We will now specify the wave function to the case of the  $\alpha$ -cluster model. In the static case, the wave function is a Slater determinant of  $\alpha$  clusters localized at some points  $\mathbf{d}$  in space:

$$\Phi = \det\{\phi_j(\mathbf{r}_i)\}, \quad (14)$$

where

$$\phi_j(\mathbf{r}_i) = \prod_{k=1}^3 \phi_{j_k}(r_{i_k}) \quad (k=x,y,z) \quad (15a)$$

and

$$\phi_{j_k}(r_{i_k}) = \left[ \frac{\nu_k}{\pi} \right]^{1/2} \exp\left\{ -\frac{\nu_k}{2}(r_{i_k} - d_{j_k})^2 \right\} \quad (15b)$$

in oscillator units  $b_x = b_y = b_z = b = 1$ . Each orbit  $\phi_j$  is occupied by two neutrons and two protons with opposite spin orientation. The total wave function is correctly antisymmetrized but not normalized. In our previous work<sup>7</sup> we allowed only the  $\mathbf{d}$  parameters to vary in time. To make the model more realistic, one should allow also for a variation of the size of the  $\alpha$  clusters. This was shown<sup>6</sup> to be important for the dynamics in the  $\alpha + \alpha$  system. In the next section we present calculations for the  $\alpha$ -<sup>12</sup>C system which elucidate this problem.

In order to describe correctly the time evolution of the clusters, the positions  $\mathbf{d}_j$  (and the width  $\nu$ ) must be complex quantities. This can be seen most easily in the case of a uniformly traveling  $s$  wave. Starting from a wave function of the form

$$\phi = e^{i\mathbf{k}\mathbf{r}} e^{-\nu(\mathbf{r}-\mathbf{d}_R)^2/2}, \quad (16)$$

with  $\mathbf{d}_R$  real and the oscillator length  $b=1$  ( $\nu=1$  for the equilibrium configuration) we rewrite it as

$$\phi = ce^{-\nu(\mathbf{r}-\mathbf{d}_R - i\mathbf{d}_I)^2/2}, \quad (17)$$

where  $c$  is a complex factor independent of  $\mathbf{r}$ . So the wave function (16) is just an  $s$  wave with a complex position  $\mathbf{d} = \mathbf{d}_R + i\mathbf{d}_I$ , where the imaginary part is related to the momentum  $\mathbf{d}_I = b^2\mathbf{k}$ .

For the calculation of the various quantities entering Eq. (7), the standard  $\alpha$ -cluster model technique<sup>5</sup> can be applied. One obtains, e.g., the expression for the norm:

$$\mathcal{N} = (\det n_{ij})^4, \quad (18)$$

where

$$n_{ij} = \prod_{k=1}^3 n_{i_k j_k} \quad (19)$$

and

$$n_{i_k j_k} = \frac{\lambda_k}{\pi} \exp\left\{ -\lambda_k^2 (d_{i_k}^* - d_{j_k})^2 / 4 \right\}, \quad (20)$$

with

$$\lambda_k = \left[ \frac{2\nu_k \nu_k^*}{\nu_k + \nu_k^*} \right] \quad (k=x,y,z). \quad (21)$$

With an adequate choice of the interaction, the calculation of  $S_{\alpha\beta}$  and  $\partial_{\mathbf{d}_\alpha}(\mathcal{H}\mathcal{N}^{-1})$  in Eq. (7) is almost analytical, involving just a numerical inversion of the overlap matrix.

### D. Time evolution of parity-projected wave functions

The TDCM formalism for multideterminantal wave functions is capable of describing states which possess complicated symmetries, like, e.g., angular momentum projected states. However, the treatment of such states in a time-dependent formalism is a tedious job. Thus, we restrict ourselves in this paper to the simplest example of parity-projected states. The wave function in this case is

$$\Phi(\mathbf{r};t) = \sum_{i=1}^8 f_i \bar{\Phi}_i(\mathbf{r};t), \quad (22a)$$

with

$$\bar{\Phi}_i(\mathbf{r},t) = \hat{\Pi}_i \Phi(\mathbf{r};t), \quad (22b)$$

where

$$\hat{\Pi}_i = (\hat{\Pi}_x)^{n_{x_i}} (\hat{\Pi}_y)^{n_{y_i}} (\hat{\Pi}_z)^{n_{z_i}} \quad (n_{k_i} = 0,1), \quad (22c)$$

with

$$\hat{\Pi}_x \Phi(x;t) = \Phi(-x;t), \quad (22d)$$

and  $f_i$  equals  $-1$  or  $+1$ . Using Eq. (22) we can describe the evolution of parity eigenstates of the total system

$$\Phi^{(\pm)} = (1 \pm \hat{\Pi}_x \hat{\Pi}_y \hat{\Pi}_z) \Phi. \quad (23)$$

Since the parity operator commutes with the Hamiltonian, the parity of the total system is conserved during the time evolution.<sup>1</sup> It is extremely difficult to assure the parity conservation for each subsystem (fragment) separately. In general, it is possible only if the parity operators for the individual fragments commute with one of the symmetry operators of the total Hamiltonian. This is exceptional, and thus in most cases parity conservation for the fragments results from the hidden dynamical symmetry of the system. As an example of such a symmetry one can consider a special configuration of four  $\alpha$  clusters. Let three of them form an equilateral triangle with one of its sides parallel to the  $x$  axis and with the center of gravity at the origin. If the fourth  $\alpha$  particle is put on the  $z$  axis ( $x=y=0$ ), then the parity-projected states of a <sup>12</sup>C nucleus are obtained by acting with the operator  $(1 \pm \hat{\Pi}_y)$  on the wave function of the total system. Obviously,  $\hat{\Pi}_y$  commutes with both  $\hat{\Pi} = \hat{\Pi}_x \hat{\Pi}_y \hat{\Pi}_z$  and  $\hat{H}$ . Hence, we have a dynamical symmetry, and the intrinsic parity of <sup>12</sup>C will be conserved. Some numerical examples for this case will be shown in the next section.

Each Slater determinant in expression (21) is given by Eq. (14). Consequently, the calculation of various  $A, B, \mathcal{N}, \mathcal{H}^{(i)}$  terms entering Eq. (10) is as simple as in the case of a single Slater determinant discussed above. Hence, e.g., expression (18) for the norm contains now

$$n_{i_k j_k} = \frac{\lambda_k}{\pi} \exp\{-\lambda_k^2 (d_{i_k}^* - q_{j_k})^2 / 4\}, \quad (24)$$

where  $\lambda_k$  is given by Eq. (21) and  $\mathbf{q}_j = \mathbf{f}_j \mathbf{d}_j$ .

### E. Choice of the independent variables

An evolution of the wave packet (14) for  $N$  clusters is parametrized by  $3N$  coordinatelike and  $3N$  momentum-like parameters. Moreover, the variation of the size of the clusters introduces in addition three coordinates and three momenta. Thus, the number of coupled Euler-Lagrange equations for the dynamical parameters becomes rather large already in medium-heavy nuclei. However, one can sometimes choose an initial configuration of the system which exhibits an additional symmetry. An example of that kind was given in subsection D for the  $\alpha$ - $^{12}\text{C}$  system. Out of the total number of 30 variables in this special case, only 10 are independent variables. An analysis of the dynamical symmetries for each system under consideration allows one to select optimal initial evolution conditions such that the number of independent variables for the system is reduced. One should remark that though such initial evolution conditions are very special, they are nevertheless not misleading. The properties of the TDCM trajectory, the kinetic energy of the fragments, the energy dissipation, or the reaction mechanism change continuously while removing the dynamical symmetry.

The separation of the c.m. motion from the total evolution is only a particular example of linear dependences among the dynamical variables. Since  $\sum_i d_{i_k} = c(k)$ , with  $c(k)$  complex and constant in time, one may transcribe the initial set of equations in terms of relative and c.m. variables. In this way, the c.m. separates trivially, and the number of coupled equations is reduced.

## III. RESULTS FOR THE $\alpha$ - $^{12}\text{C}$ REACTION

The first TDCM calculations for the  $\alpha$ - $^{12}\text{C}$  reaction were reported in Ref. 7. In that paper we discussed the restricted parametrization of the wave function in terms of frozen  $\alpha$  clusters. Here we want to add those degrees of freedom which are consistent with the cluster description of nuclei and which may provide a convenient way of storing excitation energy in intrinsic degrees of freedom of the system. The qualitative properties of light-ion dynamics are also expected to depend strongly on these new degrees of freedom.

It is commonly believed that the first excited  $0^+$  state of  $^4\text{He}$  at  $E^* = 20.1$  MeV is the breathing mode. On the other hand, the collective quadrupole strength is expected to be concentrated in an excitation energy range well above the binding energy of  $^4\text{He}$ . Hence, the breathing mode seems to be the most favorable collective mode of  $\alpha$  particles. In fact, the properties of  $\alpha$  clusters in light  $4N$  nuclei may differ somewhat from those of free  $\alpha$  particles. Nevertheless, as far as the cluster picture of light nuclei makes sense, and one has indeed several convincing arguments to support this picture, it is plausible to assume that the breathing (monopole) mode is a more important way of storing excitation energy than the quadrupole mode. To test this assumption, we have performed two

kinds of TDCM calculations, allowing either only for spherical clusters of variable size (the monopole mode) or for variations of both the radius and  $\beta$ -quadrupole deformation ( $\beta = v_z/v_x$ ) of the clusters. We have found that the qualitative features of the  $\alpha$ - $^{12}\text{C}$  trajectories at low energies ( $E_{\text{c.m.}} < 30$  MeV) are the same in the two approximations, and the amount of energy stored in intrinsic excitations hardly differs in both cases. Thus, in the following presentation we have restricted the TDCM calculations to variations of the radius of spherical clusters only.

For central collisions of  $^4\text{He}$  and  $^{12}\text{C}$ , we have performed calculations with frozen and variable cluster sizes. Figure 1 presents the results at  $E_{\text{c.m.}} = 4$  MeV. At  $t=0$ ,  $^{12}\text{C}$  has the configuration of an equilateral triangle, and the incoming  $^4\text{He}$  moves along the line perpendicular to the  $^{12}\text{C}$  plane, crossing that plane in the center of gravity of  $^{12}\text{C}$ . The two upper figures exhibit results obtained in the frozen-cluster approximation. The upper left curve shows the distance  $d_\alpha$  between the  $\alpha$  particle and the  $^{12}\text{C}$  plane as a function of time. The upper right curve gives the time dependence of the distance  $\Delta_c$  of the center of gravity in  $^{12}\text{C}$  from the bottom side of the  $^{12}\text{C}$  triangle. (During the evolution,  $|\Delta_c|$  equals  $\sqrt{3}/2$  times the side length of the  $^{12}\text{C}$  triangle.) At  $t=0$ ,  $\Delta_c$  is chosen to be negative. A change of sign of  $\Delta_c$  at some later time means the reflection of the initial configuration of  $^{12}\text{C}$  with respect to an axis  $O_x$  which passes through the center of  $^{12}\text{C}$  and is parallel to the bottom side of the triangle. The upper two curves in Fig. 1 exhibit the reflection of the incoming  $\alpha$  particle from the  $^{12}\text{C}$  nucleus. The reaction is accompanied in the initial phase by a strong reduction of the size of  $^{12}\text{C}$ . In the final state,  $^{12}\text{C}$  shows small amplitude oscillations, and  $^4\text{He}$  moves backwards. The two lower curves in Fig. 1 show a complicated time dependence of  $d_\alpha$  and  $\Delta_c$  which is typical for a fusion event. These results have been obtained with allowing for a variable size of the  $\alpha$  clusters. One may notice that the

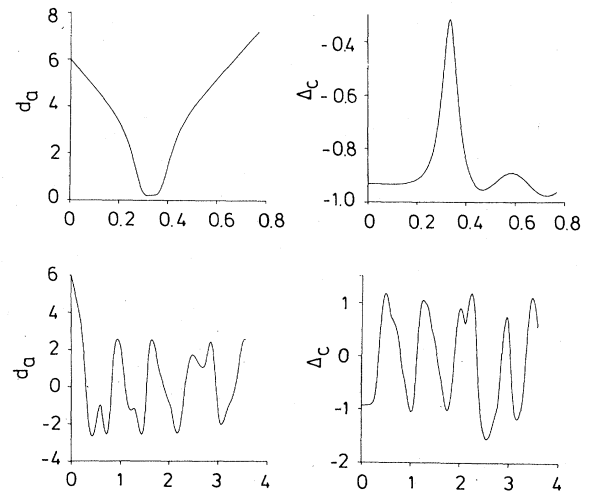


FIG. 1. A comprehensive representation of the  $\alpha$ - $^{12}\text{C}$  reaction at  $E_{\text{c.m.}} = 4$  MeV and impact parameter equal to zero.  $d_\alpha$  and  $\Delta_c$  are given in fm, whereas the time step is  $10^{-21}$  sec. For details see the description in the text.

incoming  $\alpha$  particle oscillates around the center of  $^{12}\text{C}$  and, at the same time, the  $\alpha$  clusters of  $^{12}\text{C}$  perform complicated vibrations which tend to restore the reflection symmetry of  $^{12}\text{C}$  with respect to the axis  $O_x$ , i.e., the position of each cluster in  $^{12}\text{C}$  is frequently reflected at the axis  $O_x$ .

In the TDCM we are also able to perform the parity projection of the total wave function. Figure 2 shows the time evolution of  $d_\alpha$  and  $\Delta_c$  for the parity projected wave function of the  $\alpha$ - $^{12}\text{C}$  system in the approximation with variable cluster sizes. The excitation energy of the system is again 4 MeV, as in Fig. 1. The upper two curves show results for the positive parity wave function of the system. Results for negative parity are shown in the two lower figures. One notices that the time evolution of the positive parity wave function does not substantially differ from the corresponding evolution of wave functions without well-defined parity which was shown at the bottom of Fig. 1. The evolution of the negative parity wave function, however, exhibits qualitative differences compared to both the positive parity and mixed parity evolutions. In all these calculations,  $^4\text{He}$  and  $^{12}\text{C}$  fuse, which suggests that the parity projection is less important for energy dissipation than a variable size of the clusters. This property is intuitively expected, as the parity projection does not correspond to a new degree of freedom, but rather to a new physical condition imposed on the time evolution of the classical Hamiltonian system, and hence it may be significant for the properties of the final states. Indeed, Fig. 3 shows an example for this significance for a central collision of  $^4\text{He}$  and  $^{12}\text{C}$  at  $E_{\text{c.m.}} = 14$  MeV. The upper-most figures present  $d_\alpha(t)$  and  $\Delta_c(t)$  in the approximation of frozen  $\alpha$ -cluster radii. In this approximation, the  $\alpha$  particle passes through the  $^{12}\text{C}$  plane, depositing a large amount of energy in  $^{12}\text{C}$ . This energy cannot be stored in the intrinsic excitations of  $^{12}\text{C}$ , and hence it explodes.

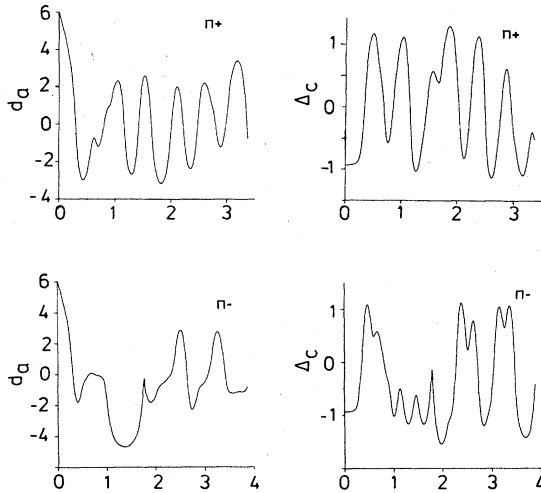


FIG. 2. Same as in Fig. 1, but for positive ( $\Pi^+$ ) and negative ( $\Pi^-$ ) parity wave functions of the  $\alpha$ - $^{12}\text{C}$  system. For details see the description in the text.

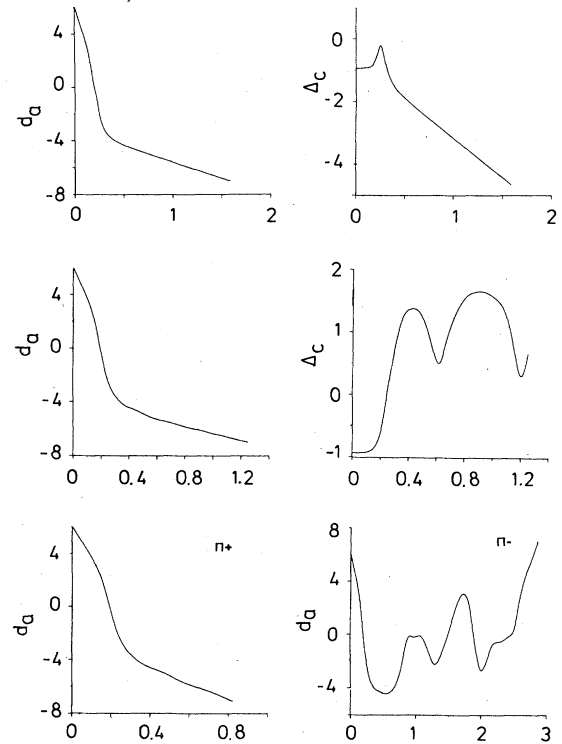


FIG. 3. Same as in Figs. 1 and 2, but for  $E_{\text{c.m.}} = 14$  MeV. For more details see the description in the text.

The inclusion of variations of the  $\alpha$ -cluster radii (the two curves in the middle of Fig. 3) does not change the energy transferred to  $^{12}\text{C}$ , but it prevents the explosion of  $^{12}\text{C}$  after the reaction. Therefore one observes a large amplitude oscillation of  $^{12}\text{C}$ . The effect of the parity projection can be seen at the bottom of Fig. 3. The left bottom curve shows  $d_\alpha(t)$  for the positive parity wave function. This curve resembles closely the one obtained before without parity projection, although now the energy deposited in the  $^{12}\text{C}$  target is smaller. Obviously,  $^{12}\text{C}$  remains bound after the reaction. For the negative parity wave function (bottom right of Fig. 3), the situation is, however, very different. The  $\alpha$  particle penetrates a few times into the target and is finally pushed backwards with a velocity close to the initial velocity. In general, we find that the parity projection does not significantly influence the amount of energy which can be stored in the intrinsic excitations. Therefore, it will be less important for a quantitative determination of the fusion window. On the contrary, the parity projection modifies the ion-ion potential so that the angular distributions and final velocities of the reaction products may differ from those obtained for mixed-parity time evolutions.

#### IV. RESULTS FOR THE $^{12}\text{C}$ - $^{12}\text{C}$ REACTION

This section will be devoted to the analysis of the reaction between two  $^{12}\text{C}$  nuclei. We emphasize particularly the TDCM calculation of the fusion excitation function

which can be compared with the experimental data, thus providing a serious test for the dissipation and randomization mechanisms in our model. The  $^{12}\text{C}$ - $^{12}\text{C}$  reaction was never studied extensively within the TDHF approximation. To our knowledge, Maruhn and Cusson<sup>19</sup> were the only ones who studied this reaction, but their calculations were restricted to central collisions and assumed spherical nuclei. There are probably several reasons for this lack of calculations. It is known that  $^{12}\text{C}$  is deformed in the ground state. However, in the filling approximation which is commonly used to deal with partially filled shells, one obtains instead spherical fragments. In such "classical" evolution equations like those of TDHF or the TDCM, the deformation of ions increases the influence of the initial geometrical configuration of the fragments on the allowed final states. Moreover, one expects that the spurious c.m. excitations in TDHF can be important for  $^{12}\text{C}$  nuclei. All these problems can be better addressed in the TDCM.

#### A. Fusion excitation function

The configuration of C ions in the initial state does not prohibit various binary reactions leading to the breakup of the projectile and, consequently, to various incomplete fusion or deep-inelastic events. In the next section, a more systematic discussion of these possible reactions will be presented for the  $^{12}\text{C}$ - $^{16}\text{O}$  system. In principle, we can identify different binary processes by evolving the  $^{12}\text{C}$ - $^{12}\text{C}$  system for a sufficiently long time. Hence, we can in

principle separate the fusion reaction leading to  $^{24}\text{Mg}$  from any other process. Unfortunately, the measurement of the fusion excitation function is not free from those inaccuracies which are related to a clear-cut distinction between various "fusionlike" events. Consequently, in experiment one has to use an operational definition of fusion. In Ref. 20, for example, one defines as fusion all events registered by the fusion telescope for which the charge is greater than the charge of the heavier ion. Hence the experimental fusion excitation function should be compared to the calculated one only at bombarding energies for which projectile breakup processes constitute an insignificant fraction of the total cross section, i.e., at low energies.

The equilibrium configuration of  $^{12}\text{C}$  in the cluster model calculation is given by an equilateral triangle with a distance of 3.335 fm between the  $\alpha$  particles. The strong clustering for the  $B1$  force leads to this large separation of the  $\alpha$  particles and, consequently, to an rms radius which is 10% larger than the experimental one. Figure 4 shows the calculated fusion excitation function for two different approximations. In the first one, we evolve  $^{12}\text{C}$  ions for frozen diameters of the  $\alpha$  clusters [ $v_k(t) = v_k(t=0)$ ,  $k=x,y,z$ ]. Results for this approximation are shown by open circles in Fig. 4. In the second approximation, we allow the parameters  $v_x, v_y, v_z$  to vary independently in time (open triangles in Fig. 4). The  $^{12}\text{C}$  ions are put in two different parallel planes which move towards each other along the line perpendicular to these planes. At  $t=0$  the two nuclei are separated by 10 fm.

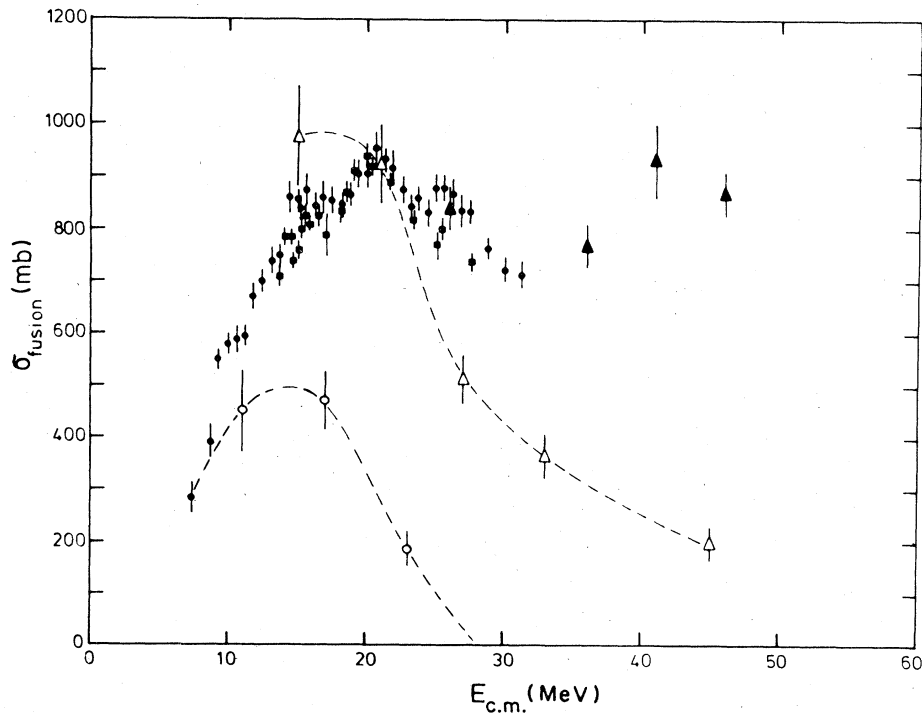


FIG. 4. The fusion excitation function for the  $^{12}\text{C}$ - $^{12}\text{C}$  system as a function of the c.m. energy. The experimental data are taken from Refs. 20 (full circles), 21 (full squares), and 22 (full triangles). The theoretical results were obtained with frozen (open circles) or variable (open triangles) cluster size. The dashed lines are to guide the eye.

In this initial configuration, the mutual Coulomb interaction between the two nuclei is still important, even though the nuclear interaction is negligible. This has to be taken into account when determining the asymptotic energy and impact parameter at  $t \rightarrow -\infty$ . In the actual calculations we have determined the Coulomb interaction at a distance of twice the rms radius of  $^{12}\text{C}$  and have matched a Rutherford trajectory to the calculated time evolution at this point.

Variations of  $\nu$  do not show a significant influence on the critical angular momentum for fusion ( $l_{>} \simeq 12\hbar \pm 1.5\hbar$  in both approximations) but strongly decrease the lower off  $l_{<}$  for fusion. Thus, the  $\nu$  variations help to open the fusion window. In the preceding section this was already demonstrated for the headon collision of an  $\alpha$  particle with  $^{12}\text{C}$ . The experimental data on the fusion excitation function in Fig. 4 have been taken from the recent works from Saclay,<sup>21</sup> Argonne,<sup>20</sup> and Virginia.<sup>22</sup> The experimental points at  $E_{\text{c.m.}} < 12$  MeV are in excellent agreement with the calculated points for the variable- $\nu$  approximation. The fall of the calculated  $\sigma_{\text{fus}}(E_{\text{c.m.}})$  beyond 25 MeV is due to the increased presence of incomplete fusion events for  $^8\text{Be}$  and  $\alpha$  capture. These processes have been systematically excluded from the calculated  $\sigma_{\text{fus}}$ . In the frozen- $\nu$  approximation the incomplete fusion events appear at lower excitation energies, but the qualitative pattern of the  $^{12}\text{C}$ - $^{12}\text{C}$  reaction remains unchanged. In the neighboring  $^{12}\text{C}$ - $^{16}\text{O}$  system at  $E_{\text{c.m.}} = 25$  MeV, we find  $l_{>} = 16\hbar$ , which agrees exactly with the TDHF result for the same energy.<sup>14</sup> Hence, in spite of different foundations and a different two-body force in the two methods, the TDHF and TDCM calculations seem to agree rather well. At least below the threshold for incomplete fusion processes, we do not notice a shortage of degrees of freedom in the cluster model wave function.

We have also checked the influence of the initial geometrical configuration of  $^{12}\text{C}$  on the calculated  $l_{>}$  and  $l_{<}$ . For that we have calculated the TDCM trajectories at energies of 11 and 17 MeV for two  $^{12}\text{C}$  ions which are

placed on parallel planes and move along a direction which is also parallel to these planes. The calculated limiting angular momenta  $l_{<}, l_{>}$  for fusion in this configuration are  $l_{<} = 2\hbar$ ,  $l_{>} = 7\hbar$  and  $l_{<} = 3\hbar$ ,  $l_{>} = 9\hbar$ , respectively, at these two energies, in agreement with the results for the other configuration. Moreover, we have found that parity projection for both kinds of geometrical configurations is insignificant, at least as far as  $l_{<}$  and  $l_{>}$  are concerned.

### B. Molecular configurations

The observation of dramatic structures in excitation functions for elastic scattering of  $^{12}\text{C}$ - $^{12}\text{C}$  (Ref. 23),  $^{12}\text{C}$ - $^{16}\text{O}$  (Ref. 24), and  $^{16}\text{O}$ - $^{16}\text{O}$  (Ref. 25) has led to a tremendous amount of experimental and theoretical activity in recent years.<sup>26</sup> The broad structures in these excitation functions are generally taken to arise from molecular (or shape) resonances. Most of these resonance structures have been seen in systems in which at least one of the partners is C or O. This suggests a significant role of clustering in the formation mechanism of these structures since it is known that in C and O nuclei  $\alpha$  clustering plays a significant role both in the structure of low-lying states and in the decay pattern. Here we present an example of such a molecular configuration for two  $^{12}\text{C}$  nuclei at an angular momentum of  $l = 10\hbar$  and a c.m. energy of 17 MeV (see Fig. 5). Experimentally, close to this energy a large number of  $10^+$  resonances have been found.<sup>27</sup> This estimate of the excitation energy should be taken as an approximate one since we have not requantized the TDCM action functional for the orbiting motion of Fig. 5.<sup>28</sup> The plot in Fig. 5 represent the  $yz$  cut of the equidensity surfaces. The equidensity contours are drawn in steps of 10% of the maximal density in the initial state at  $t = 0$ . The unit distance along the  $y$  and  $z$  axes is 1 fm. At  $t = 0$ , the  $\alpha$  particles in each ion are pushed towards each other uniformly along the  $z$  axes. The  $^{12}\text{C}$  ions in the initial configuration are put into two parallel planes which

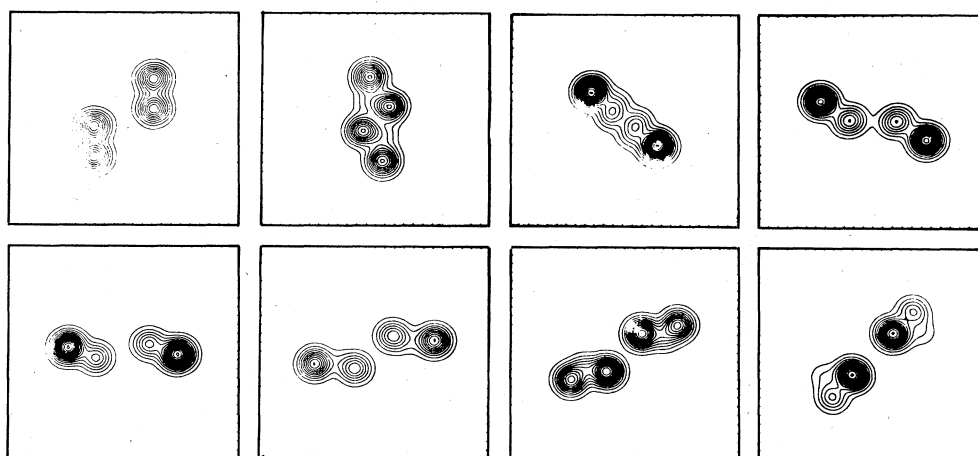


FIG. 5. Equidensity contour plots for the  $^{12}\text{C}$ - $^{12}\text{C}$  reaction with a c.m. energy of 17 MeV and an angular momentum of  $10\hbar$ . The size of each frame is 24 fm. The contour plots are shown at times 0.2, 0.6, 0.9, 1.1, 1.3, 1.5, 1.7, and  $1.9 \times 10^{-21}$  sec (left to right, upper row first) after the start. The contour lines are drawn in steps of 10% of the maximum density in the initial configuration.

are separated by 10 fm. In each  $^{12}\text{C}$  nucleus in the initial configuration, the  $\alpha$  particles are situated out of the  $yz$  plane. Consequently, the plots in Fig. 5 show only four instead of six density centers. Notice in Fig. 5 that the strong  $\alpha$  clustering leads to the relatively large separation distance between the  $^{12}\text{C}$  ions in the later states of the process. Thus, the two  $^{12}\text{C}$  nuclei move as almost separate entities in the common intermolecular potential, and their separation distance is  $\sim 8$  fm. In a recent analysis of all known  $^{12}\text{C} + ^{12}\text{C}$  resonances by Bromley and Erb<sup>29</sup> in terms of a local potential, an average separation of  $\sim 7$  fm was deduced. This close agreement further supports the interpretation of our state as a molecular resonance.

### V. RESULTS FOR THE $^{12}\text{C}$ - $^{16}\text{O}$ REACTION

In the preceding section we have shown results for the symmetric reaction between two  $^{12}\text{C}$  ions. In this section we want to remove this projectile-target mass symmetry. For that the  $^{12}\text{C} + ^{16}\text{O}$  reaction is investigated in some detail. This reaction was studied before by Krieger and Davies<sup>14</sup> using the TDHF method in the two-dimensional rotating-frame approximation<sup>30</sup> with the local version of the Skyrme force. The initial configuration of O and C was prepared in the filling approximation. In Ref. 14, the main emphasis was placed on calculation of the fusion excitation function. In contrast, we concentrate on various incomplete and deep-inelastic processes in this system as found in our TDCM calculations. We recall from the preceding section only that  $l >$  as calculated in Ref. 14 agrees with the TDCM estimate.

The classification and microscopic description of various reaction mechanisms in the collision of two energetic heavy ions is far from being complete. In recent years, much emphasis was put on both incomplete fusion and deep-inelastic reactions besides the fusion reaction. Incomplete fusion is the name given to fast binary processes in which part of the projectile fuses with the target while the remaining ejectile is emitted with approximately the beam velocity, preferentially in forward direction. Experimental studies of these processes have involved strongly mass-asymmetric target-projectile combinations with heavy target nuclei. Whether or not similar processes occur for less asymmetric combinations and (or) for light ions still remains an open question. The name deep inelastic is given to reactions in which the kinetic energy of the colliding ions is dissipated into intrinsic excitations.

Hence, these processes are believed to happen on a slower time scale than the incomplete fusion processes. (For a detailed discussion of this subject we refer the reader to the recent review articles by Gerschel and Siemssen.<sup>31</sup>)

Recent studies of Siwek-Wilczyńska *et al.*<sup>9</sup> point to the threshold behavior of the incomplete fusion reaction which can be explained with a bin-type model.<sup>9,32</sup> The extension of this model is the "sum-rule" model of Wilczyński *et al.*<sup>10</sup> which classifies the incomplete fusion reactions as a subgroup of angular momentum matched binary reactions. Using the generalized concept of critical angular momentum, Wilczyński *et al.*<sup>10,33</sup> point to the angular momentum selectivity of the final state. However, new results obtained by the Orsay group from collisions on spherical targets at low bombarding energies<sup>34</sup> put in question certain aspects of the critical distance concept in the "sum-rule" model. Nevertheless, this model still provides the basic frame for classifying the existing data on binary reaction processes. Hence, the results of this section will be discussed in the context of this model.

The advantage of the TDCM is its potential to describe a much more realistic initial geometry of the reaction between light nuclei than is the case for TDHF calculations. For the deterministic time evolution of the wave function in the TDHF method the symmetry imposed on the initial condition influences properties of the final state and, in many cases, may even prohibit the existence of physically significant configurations. Unfortunately, this is a drawback for all initial value methods in a restricted manifold of the full Hilbert space. Hence, in semiclassical investigations of heavy ion dynamics, less restrictive initial conditions are so important.

Results for the  $^{12}\text{C}$ - $^{16}\text{O}$  system shown in this section have been obtained in the frozen cluster approximation [ $\psi(t) = \psi(t=0)$ ]. This restriction obviously influences the threshold angular momenta for various incomplete fusion processes, but does not change the qualitative features of the C-O dynamics. In all calculations the Coulomb force is treated exactly, and the matching to the Rutherford trajectory in the interaction region is the same as described before in Sec. IV A.

Figure 6 shows the  $yz$  equidensity plots for the  $^{12}\text{C}$ - $^{16}\text{O}$  reaction with a c.m. energy of 26 MeV and an angular momentum of  $12.9\hbar$ . As in the preceding section, the time evolution is started with an initial distance of 10 fm between the nuclei, from which the  $\alpha$  particles in C and O are pushed uniformly towards each other. The density

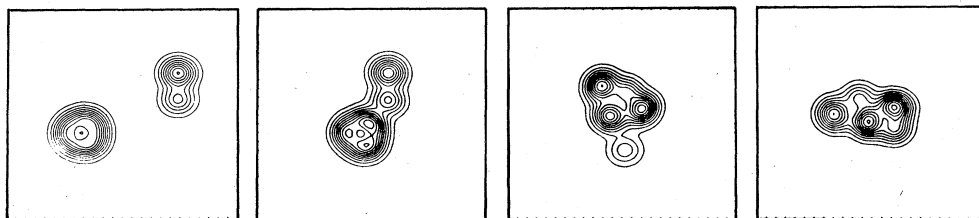


FIG. 6. Same as Fig. 5 for the  $^{12}\text{C}$ - $^{16}\text{O}$  reaction with a c.m. energy of 26 MeV and an angular momentum of  $12.9\hbar$ . The contour plots are shown at times 0.0, 0.3, 0.6, and  $0.9 \times 10^{-21}$  sec (left to right).

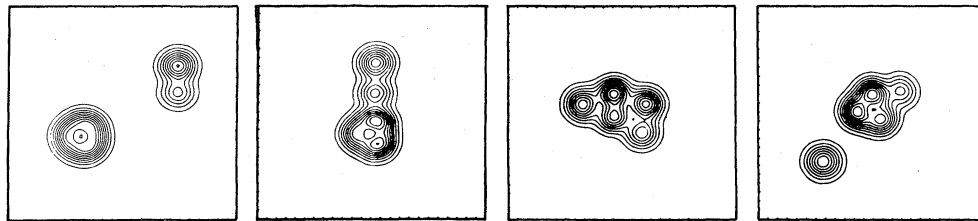


FIG. 7. Same as Fig. 5 for the  $^{12}\text{C}-^{16}\text{O}$  reaction with a c.m. energy of 26 MeV and an angular momentum of  $15.5\hbar$ . The contour plots are shown at times 0.0, 0.4, 0.8, and  $1.2 \times 10^{-21}$  sec (left to right).

contours in Fig. 6 are plotted until  $t = 0.9 \times 10^{-21}$  sec, when the two nuclei have fused. For longer times, we find no evidence for either breakup or fission of the compound system. At slightly higher angular momentum, one begins to observe nonfusion events. An example is shown in Fig. 7, where we show the C-O collision at the same energy for  $l = 15.5\hbar$  which leads to incomplete fusion.  $^{12}\text{C}$  and  $^{16}\text{O}$  approach each other, and at  $t \approx 10^{-21}$  sec an  $\alpha$  particle is emitted in the  $yz$  plane with a velocity approximately equal to the beam velocity. At still higher angular momentum,  $^{16}\text{O}$  fuses with only one  $\alpha$  particle, and a  $^8\text{Be}$  nucleus (which may disintegrate into two  $\alpha$  particles) is emitted. Such a process is shown in Fig. 8 for  $l = 18.2\hbar$  and an energy of 46 MeV. Here, two  $\alpha$  particles are emitted out of the  $yz$  plane for  $t \approx 0.45 \times 10^{-21}$  sec after the start of the motion of the C and O nuclei. The remaining nucleus forms an excited  $^{20}\text{Ne}^*$  nucleus. Finally, at  $l = 24.1\hbar$  (and an energy of 76 MeV) the complete breakup of the projectile into three  $\alpha$  particles is seen in Fig. 9. One  $\alpha$  particle is moving approximately in the  $yz$  plane, whereas the two other ones move out of the reaction plane in a symmetric way (one above, one below the plane). Their density in the  $yz$  plane is therefore rather small, and in the figure they cannot be seen for longer times.

The time evolution in Figs. 6–9 shows some kind of  $l$  selectivity for different binary reactions in the  $^{12}\text{C}-^{16}\text{O}$  system as suggested by Wilczyński *et al.*<sup>9,10</sup> However, the picture that emerges from our TDCM calculations seems to be more complicated than this model. We notice an equally important role of the total c.m. energy of the system in addition to the total angular momentum in selecting a specific binary reaction. At  $l = 12.9\hbar$ ,  $E_{\text{c.m.}} = 26$  MeV, the C-O system fuses, as shown in Fig. 6. However, for a more central collision at the same angular momentum ( $E_{\text{c.m.}} \approx 36$  MeV), we find an inelastic scattering of  $^{12}\text{C}$  and  $^{16}\text{O}$  with an exchange of one  $\alpha$  particle between

the two reaction partners. Similarly, at  $l = 14.5\hbar$  the peripheral C-O collision at  $E_{\text{c.m.}} = 21$  MeV leads to fusion, whereas the more central collision at  $E_{\text{c.m.}} = 46$  MeV leads to the breakup of  $^{12}\text{C}$  and to  $\alpha + ^{24}\text{Mg}^*$  in the final state. At the even higher angular momentum  $l = 18\hbar$ , the peripheral collision at  $E_{\text{c.m.}} = 26$  MeV leads to inelastic collision, whereas the more central collision at  $E_{\text{c.m.}} = 60$  MeV leads again to breakup of  $^{12}\text{C}$ , this time into an  $\alpha$  particle and a loosely bound  $^8\text{Be}$  nucleus. Hence, the TDCM calculations do not provide a clear cut confirmation of the threshold behavior of incomplete fusion reactions as proposed by Siwek-Wilczyńska *et al.*<sup>9,10,31</sup> We find in the TDCM that the ejectile remaining after an incomplete fusion process is emitted with approximately the beam velocity. However, this happens only in peripheral collisions. This would tentatively suggest a peripheral nature of incomplete fusion processes.

## VI. CONCLUSIONS

An explanation and understanding of various exotic phenomena found in collisions of heavy ions is still a domain left for phenomenological models. On the other hand, a fully microscopic description in terms of the underlying elementary interactions between nucleons may not become feasible in the near future. This provides a motivation for the development of semimicroscopic models which start with effective two-body interactions between the constituents and parametrize the dynamics in terms of collective variables which, moreover, have a clear semiclassical meaning. One model of this kind, the time-dependent cluster model, was used in this paper. This model has several advantages for practical applications. First of all, it allows the use of finite-range interactions like the Brink-Boeker force. Second, it can be extended easily by relaxing the constraints put on the time evolution of the dinuclear system, like the fixed size of the  $\alpha$  clusters, the particular symmetry of the initial condition,

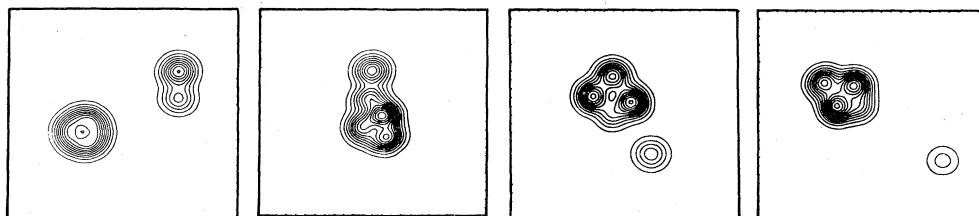


FIG. 8. Same as Fig. 5 for the  $^{12}\text{C}-^{16}\text{O}$  reaction with a c.m. energy of 46 MeV and an angular momentum of  $18.2\hbar$ . The contour plots are shown at times 0.0, 0.3, 0.6, and  $0.9 \times 10^{-21}$  sec (left to right).

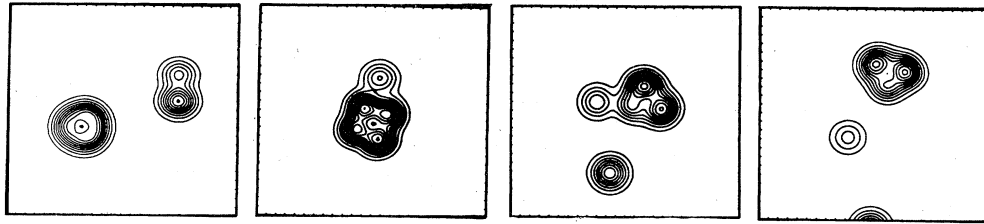


FIG. 9. Same as Fig. 5 for the  $^{12}\text{C}-^{16}\text{O}$  reaction with a c.m. energy of 76 MeV and an angular momentum of  $24.1\hbar$ . The contour plots are shown at times 0.0, 0.2, 0.4, and  $0.6 \times 10^{-21}$  sec (left to right). Compared to Figs. 6–8, the  $^{12}\text{C}$  nucleus has been rotated around the  $z$  axis by  $180^\circ$  in the initial configuration.

and/or the choice of the “elementary” constituents in the cluster wave function. Finally, one may explicitly take into account the  $\alpha$ -particle correlations which are known to be important in light nuclei and which may play a major role in the intermediate stages of the dinuclear evolution. This flexibility of the TDCM permits the systematic investigation of the importance of various intuitive assumptions about the nature of ion-ion collisions. One should stress that the exact treatment of the Pauli principle in the TDCM permits the exchange of nucleons between different clusters. With the simplified wave function of the TDCM we are also able to treat multideterminantal wave functions. An example for this was shown in Sec. III for the time evolution of the parity projected wave function of the  $\alpha$ - $^{12}\text{C}$  system. In the calculations we found a rich variety of final states and complicated intermediate states. These include a molecular configuration of  $^{24}\text{Mg}$  at  $I \approx 10\hbar$ , various incomplete fusion and deep-inelastic events,  $\alpha$ -particle transfer, etc. On a quantitative level, we can even reproduce the fusion cross section at low bombarding energies below the threshold for incomplete fusion processes. (At higher energies, one should add the contribution of incomplete fusion reactions to the total fusion cross section since these processes are also summed up in the present experiments.)

Most of the experimental data concerning complete and incomplete fusion of heavy ions were successfully sys-

tematized using the “bin-type” or “sum-rule” model of Wilczyński *et al.*<sup>2,10,32</sup> Even though certain aspects of these models may be questionable, one generally believes that the concept of critical angular momentum remains valid. Our qualitative discussion in the TDCM framework (Sec. V) confirms the general features of the “bin-type” model, and moreover points out the equally important role of the c.m. energy in selecting the dominant reaction mechanism. We leave this problem for further discussion in a separate publication.<sup>35</sup>

The TDCM formalism discussed in this paper allows us to speak about the evolution of multideterminantal states as, e.g., angular momentum projected states. This possibility, which remains an intriguing prospect for future studies, would bring the calculations closer to the physical situation, thus allowing us to close the gap between phenomenological models and a future microscopic theory of heavy-ion reactions.

#### ACKNOWLEDGMENTS

We are indebted to S. Drożdż and J. Okolowicz for stimulating discussions. Two of us (W. B. and M. P.) are grateful for the hospitality of the Theory Group of the CRN Strasbourg which made this collaboration possible. M. P. also wants to thank the Danish Research Council for support.

\*Present address: Centre National d'Etudes des Télécommunications/PAA/TIM/MTI, F-92131 Issy-les-Moulineaux, France.

<sup>1</sup>S. E. Koonin, *Prog. Part. Nucl. Phys.* **4**, 283 (1980).

<sup>2</sup>J. W. Negele, *Rev. Mod. Phys.* **54**, 913 (1982).

<sup>3</sup>K. T. R. Davies, K. R. S. Devi, S. E. Koonin, and M. R. Strayer, in *Treatise on Heavy-Ion Science*, edited by D. A. Bromley (Plenum, New York, 1985), Vol. 3.

<sup>4</sup>A. Bohr and B. R. Mottelson, *Nuclear Structure* (Benjamin, New York, 1975), Vol. II.

<sup>5</sup>D. M. Brink, in *Many-Body Description of Nuclear Structure and Reactions, Proceedings of the International School of Physics, “Enrico Fermi,” Course XXXVI*, edited by C. Bloch (Academic, New York, 1966), p. 247.

<sup>6</sup>S. Drożdż, J. Okolowicz, and M. Ploszajczak, *Phys. Lett.* **109B**, 145 (1982).

<sup>7</sup>E. Caurier, B. Grammaticos, and T. Sami, *Phys. Lett.* **109B**, 150 (1982).

<sup>8</sup>D. M. Brink and E. Boeker, *Nucl. Phys.* **A91**, 1 (1967).

<sup>9</sup>K. Siwek-Wilczyńska, E. H. du Marchie van Voorthuysen, J. van Popta, R. H. Siemssen, and J. Wilczyński, *Nucl. Phys.* **A330**, 150 (1979).

<sup>10</sup>J. Wilczyński, K. Siwek-Wilczyńska, J. van Driel, S. Gonggrijp, D. C. J. M. Hageman, R. V. F. Janssens, J. Lukasiak, R. H. Siemssen, and S. Y. van der Werf, *Nucl. Phys.* **A373**, 109 (1982).

<sup>11</sup>A. K. Kerman and S. E. Koonin, *Ann. Phys. (N.Y.)* **100**, 332 (1976).

<sup>12</sup>A. B. Volkov, *Nucl. Phys.* **74**, 33 (1965); *Phys. Lett.* **12**, 118 (1964).

<sup>13</sup>J. Žofka and G. Ripka, *Nucl. Phys.* **A168**, 65 (1971); D. M. Brink, H. Friedrich, A. Weiguny, and C. W. Wong, *Phys. Lett.* **33B**, 143 (1970).

<sup>14</sup>S. J. Krieger and K. T. R. Davies, *Phys. Rev. C* **20**, 167 (1979).

<sup>15</sup>T. H. R. Skyrme, *Philos. Mag.* **1**, 1043 (1956); *Nucl. Phys.* **9**,

- 615 (1959).
- <sup>16</sup>H. Friedrich, H. Hüsken, and A. Weiguny, *Phys. Lett.* **38B**, 199 (1972).
- <sup>17</sup>S. B. Khadkikar, *Phys. Lett.* **36B**, 451 (1971).
- <sup>18</sup>W. Bauhoff, H. Schultheis, and R. Schultheis, *Phys. Lett.* **95B**, 5 (1980); **106B**, 278 (1981).
- <sup>19</sup>J. A. Maruhn and R. Y. Cusson, *Nucl. Phys.* **A270**, 471 (1976).
- <sup>20</sup>D. G. Kovar, D. F. Geesaman, T. H. Braid, Y. Eisen, W. Henning, T. R. Ophel, M. Paul, K. E. Rehm, S. J. Sanders, P. Sperr, J. P. Schiffer, S. L. Tabor, S. Vigdor, B. Zeidman, and F. W. Prosser, Jr., *Phys. Rev. C* **20**, 1305 (1979).
- <sup>21</sup>M. Conjeaud, S. Gary, S. Harar, and J. P. Wieleczka, *Nucl. Phys.* **A309**, 515 (1978).
- <sup>22</sup>R. L. Parks, S. T. Thornton, L. C. Dennis, and K. R. Cordell, *Nucl. Phys.* **A348**, 350 (1980).
- <sup>23</sup>W. Reilly, R. Wieland, A. Gobbi, M. W. Sachs, and D. A. Bromley, *Nuovo Cimento* **13A**, 897 (1973).
- <sup>24</sup>R. E. Malmin, R. H. Siemssen, D. A. Sink, and P. P. Singh, *Phys. Rev. Lett.* **28**, 1590 (1972).
- <sup>25</sup>J. V. Maher, M. W. Sachs, R. H. Siemssen, A. Weidinger, and D. A. Bromley, *Phys. Rev.* **188**, 1665 (1969).
- <sup>26</sup>D. A. Bromley, in *Nuclear Molecular Phenomena*, edited by N. Cindro (North-Holland, Amsterdam, 1978), p. 3; R. H. Siemssen, *ibid.*, p. 79; R. Könnecke, W. Greiner, and W. Scheid, *ibid.*, p. 109; Y. Abe, *ibid.*, p. 211.
- <sup>27</sup>D. R. James and N. R. Fletcher, *Phys. Rev. C* **17**, 2248 (1978).
- <sup>28</sup>E. Caurier, S. Drożdż, and M. Ploszajczak, *Phys. Lett.* **134B**, 1 (1984); *Nucl. Phys.* **A425**, 23 (1984).
- <sup>29</sup>K. A. Erb and D. A. Bromley, *Phys. Rev. C* **23**, 2781 (1981).
- <sup>30</sup>S. E. Koonin, K. T. R. Davies, V. Maruhn-Rezwani, H. Feldmeier, S. J. Krieger, and J. W. Negele, *Phys. Rev. C* **15**, 1359 (1977).
- <sup>31</sup>C. Gerschel, *Nucl. Phys.* **A387**, 297c (1982); R. H. Siemssen, **A400**, 245c (1983).
- <sup>32</sup>K. Siwek-Wilczyńska, E. H. du Marchie van Voorthuysen, J. van Popta, R. H. Siemssen, and J. Wilczyński, *Phys. Rev. Lett.* **42**, 1599 (1979).
- <sup>33</sup>J. Wilczyński, K. Siwek-Wilczyńska, J. van Driel, S. Gonggrijp, D. C. J. M. Hageman, R. V. F. Janssens, J. Lukasiak, and R. H. Siemssen, *Phys. Rev. Lett.* **45**, 606 (1980).
- <sup>34</sup>H. Tricoire, C. Gerschel, N. Perrin, H. Sergolle, L. Valentin, D. Bachelier, H. Doubre, and J. Gizon, *Z. Phys. A* **306**, 127 (1982).
- <sup>35</sup>W. Bauhoff, E. Caurier, B. Grammaticos, and M. Ploszajczak (unpublished).